Proceedings of the ASME 41th International Conference on Ocean, Offshore and Arctic Engineering OMAE2022 June 5-10, 2022, Hamburg, Germany

OMAE2022-81105

ON SIMULATING VARIABILITY OF SLOSHING LOADS IN LNG TANKS

Ronald A. Remmerswaal and Arthur E. P. Veldman*

Bernoulli Institute, University of Groningen
P.O. Box 407, 9700 AK Groningen, The Netherlands
{r.a.remmerswaal, a.e.p.veldman}@rug.nl

ABSTRACT

Local pressure measurements during liquid impacts in LNG tanks show a large variability, due to the free-surface roughness and the liquid fragmentation resulting from free-surface instabilities initiated by the gas escaping redfrom the closing gas pocket. It also makes the experimental discrimination of the effect of any multiphase parameter (density ratio, compressibility, phase transition) on impact loads more complex. The main challenges are (i) to capture both experimentally and numerically the development of the free surface instabilities; and (ii) to quantify their effect on the variability of local pressures.

Numerical modeling of the initiation of the free surface instabilities requires an accurate VOF-variant. Surface tension forces are modelled via a Young-Laplace jump condition, where the interface curvature is computed using a local height function. A parabolic interface reconstruction is required to ensure convergence of the curvature in space and time. Advection is performed with a modified EMPFA method. Spurious velocities are avoided by careful treatment of the (almost) discontinuities of the flow field. The model will be demonstrated on various simulations of breaking waves.

*Address all correspondence to this author.

1 INTRODUCTION

The use of natural gas as a fuel is considered as being transitional towards more clean energy solutions (hydrogen, solar, wind, ...). redIts transport in LNG carriers requires liquefaction of the gas at cryogenic temperatures, presenting challenges in the design of cargo containment systems. During LNG transport, using partially filled tanks, the liquid inside the container wil slosh due to irregular motions of the ship, resulting in wave impacts on the container walls. From a design point of view this presents a challenge since the structural strength is one of the key points in the design of a LNG tank: how to provide an estimate of the possible impact pressure given some sea state?

Pressure variabiity During sloshing model tests, e.g. in the Sloshel project [1], a large variability of impact pressures was observed: for carefull repetition of single impact waves, significantly different impact pressures were obtained. From this research it became clear that local effects like free surface instabilities result in a significant variability of the wave crest shape and the resulting impact pressures. Such free surface instabilities, as for example the Kelvin-Helmholtz instability, result from an inbalance of several forces: gravitational, inertial, capillary and viscous forces. Moreover such instabilities originate from

small and local perturbations to the free surface and grow (initially exponentially fast) to becoming significant deformations of the free surface, especially at the wave crest.

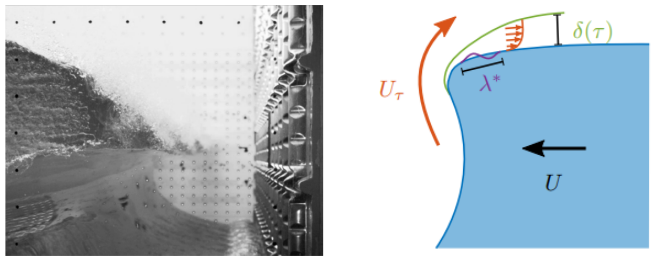

FIGURE 1. (Left) SNAPSHOT OF A BREAKING WAVE JUST BEFORE IMPACT; (right) SCHEMATIC OF ORIGIN OF INSTABILITIES.

Instabilities The role of free surface instabilities during these impacts is not well understood [1], and we will study them via computer simulation. Thus a major challenge is to use sufficient numerical damping for the simulations to remain stable, yet not so much that physical instabilities are suppressed. This requires a delicate numerical balance, which we try to achieve by keeping the numerics close to the physics of conservation laws.

The numerical modeling involves dealing with multiphase flow, featuring a multitude of jumps (discontinuities) of fluid properties across the interface separating the fluids. The thin shear layers around the interface usually are numerically underresolved and can result in unphysical interaction between the two fluids. We therefore propose to model the underresolved velocity field as being discontinuous in the direction tangential to the interface. This situation is similar to a flow modeled by the Euler equations, where contact discontinuities occur also analytically.

We explore a finite-volume numerical modeling of contact discontinuities for incompressible two-phase flow. To this end we describe the governing equations in Sect. 2, followed by our proposed discretization at the interface in Sect. 3. Not only the tangential velocity discontinuity gets attention, but also the pressure jump due to surface tension. We will show that an accurate description of the latter requires a piecewise parabolic reconstruction of the interface. Also, we demonstrate the potential of our two-phase discretization on spilling breakers. For simplicity in notation we consider a two-dimensional setting, but our simulations are three-dimensional.

2 MATHEMATICAL MODEL

The equations for *incompressible Euler flow* describe the conservation of mass and momentum in each of the phases $\pi = l, g$ (liquid and gas) in an arbitrary control volume $\omega = \omega^l \cup \omega^g$

$$\frac{\mathrm{d}}{\mathrm{d}t}\int_{\omega^\pi} \rho^\pi \,\mathrm{d}V + \int_{\partial\omega^\pi\setminus I} m_\eta^\pi \,\mathrm{d}S = 0 \tag{1}$$

$$\frac{\mathrm{d}}{\mathrm{d}t}\int_{\omega^\pi} \rho^\pi \boldsymbol{u}^\pi \,\mathrm{d}V + \int_{\partial\omega^\pi\setminus I} m_\eta^\pi \boldsymbol{u}^\pi \,\mathrm{d}S = - \int_{\partial\omega^\pi} (p^\pi - \rho^\pi \boldsymbol{g}\cdot\boldsymbol{x})\boldsymbol{\eta}\,\mathrm{d}S, \tag{2}$$

where $\boldsymbol{\eta}$ denotes the face normal, $u_\eta^\pi \equiv \boldsymbol{u}^\pi \cdot \boldsymbol{\eta}$ the normal velocity component, $m_\eta^\pi \equiv \rho^\pi u_\eta^\pi$ the mass flux through the face, p^π the pressure, ρ^π the density and $\boldsymbol{g}$ the gravitational acceleration. These equations constitute a four-equation incompressible version of the seven-equation model from [2]. For a Navier–Stokes model the effect of viscous diffusion should be included.

In incompressible flow, the mass conservation equations result in a volume constraint on the evolution of the interface

$$\frac{\mathrm{d}}{\mathrm{d}t}|\omega^l| + \int_{\partial\omega^l\setminus I} u_\eta^l \,\mathrm{d}S = 0, \tag{3}$$

where $|\omega^\pi|$ denotes the volume of ω^π. Mass conservation is applied in a primary cell, which we generically will denote by c.

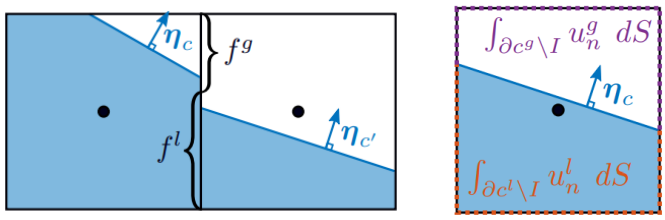

FIGURE 2. APERTURES AND SPLIT BOUNDARY INTEGRAL IN PRIMARY CONTROL VOLUMES.

The influence of surface tension, relevant in this application, is included via Laplace's law for two-dimensional surfaces:

$$-[\![p]\!] := p^g - p^l = 2\sigma\kappa. \tag{4}$$

Here κ denotes the interface mean curvature, σ the coefficient of surface tension, and $[\![p]\!]$ denotes the jump of p over the free surface. We assume immiscible fluids without phase change, and therefore $[\![u_\eta]\!] = \boldsymbol{\eta}\cdot(\boldsymbol{u}^g - \boldsymbol{u}^l) = 0$. Together with appropriate boundary conditions on $\boldsymbol{u}^\pi$ and a contact angle boundary condition on κ, this results in a closed system of equations. Note that this model does not impose any smoothness on the tangential velocity component $u_\tau = \boldsymbol{\tau}\cdot\boldsymbol{u}$, where $\boldsymbol{\tau}$ denotes the interface tangent.

Here, we consider a situation where both liquid and gas are incompressible, hence the mixture velocity field is divergence free (see Eq. (1)):

$$\int_{\partial\omega} u_\eta \,\mathrm{d}S = \int_{\partial\omega^l\setminus I} u^l_\eta \,\mathrm{d}S + \int_{\partial\omega^g\setminus I} u^g_\eta \,\mathrm{d}S = 0. \tag{5}$$

This relation forms the basis for the pressure Poisson equation, to be discussed in Sect. 3.4.

We supplement the usual pressure Poisson problem with a capillary pressure jump (4), a homogeneous Neumann boundary condition on the pressure along the side walls, and a jump condition on the normal pressure gradient at the interface:

$$\left[\!\!\left[\frac{1}{\rho}\,\partial_\eta p\right]\!\!\right] = -\left[\!\!\left[\boldsymbol{\eta}\cdot\frac{D\boldsymbol{u}}{Dt}\right]\!\!\right], \tag{6}$$

expressing a balance between the normal pressure gradient and the centrifugal force across the interface.

3 NUMERICAL MODEL

The numerical simulations are carried out on a rectangular, staggered Arakawa C-grid [3], as shown in Fig. 3. A finite-volume method is used for discretization, with the control volumes for mass conservation encadered in red, while the density ρ and the pressure p are defined in the cell centers w and e. The liquid distribution is described by a VOF-function χ which also is defined in the cell centers. The velocity components are defined at the faces of these primary cells. The green-shaded rectangle is the control volume for the momentum in x-direction, corresponding with the horizontal velocity component defined in C.

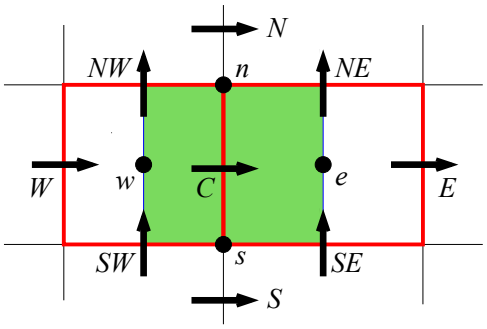

FIGURE 3. STAGGERED GRID ARRANGEMENT WITH CONTROL VOLUMES FOR MASS (RED) AND x-MOMENTUM (GREEN).

When the discretization stencils for the conservation laws are fully contained in one of the phases $\pi = l, g$, the finite-volume discretization (automatically) is conservative, so we need not spend much explanation to this (standard) case. The situation changes when these stencils cross the liquid-gas interface. This makes it a serious challenge to keep the discretization conservative for mass (liquid and gas) as well as for momentum. As mentioned in the previous section, not only the VOF function, but also the pressure and the tangential velocity feature a discontinuity across the interface. In the next subsections we will shortly describe our discretization approach to deal with these discontinuities. It has been combined with the ComFLOW simulation method for (violent) free-surface and multi-phase flows, developed at the University of Groningen in cooperation with the Technical University Delft and MARIN, and described in, e.g., [4–7].

3.1 Advection of the liquid region

Our goal is the accurate prediction of breaker tongues before impact, which requires a sharp description of the liquid surface. Therefore the liquid is advected with a geometric VOF-method based on Lagrangian considerations.

One possibility is to reconstruct the 'origin' of the contents of a primary cell at the previous time step, as in the

Lagrangian-Eulerian Advection Scheme (LEAS) [8]. This idea is sketched in Fig. 4, and makes use of a flow map Ψ which maps fluid particles from one time step to another. In mathematical terms: $\Psi^{\delta}\boldsymbol{x}(t^{(n)}) = \boldsymbol{x}(t^{(n+1)})$. Hence, the 'origin' (in mathematics called the *pre-image*) of a cell c is indicated by $\Psi^{-\delta}c$, and the amount of liquid is found by intersection with the liquid region $\Omega^{l,(n)}$.

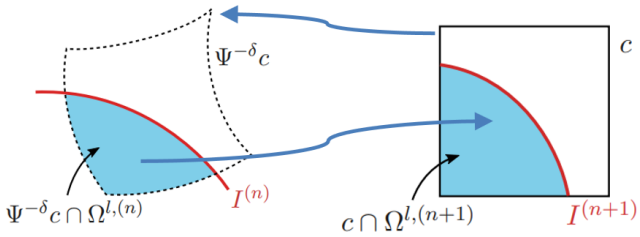

FIGURE 4. A LAGRANGIAN REMAPPING STEP RECONSTRUCTS THE CONTENTS OF A COMPUTATIONAL CELL AT THE PREVIOUS TIME STEP.

Remapping errors This Lagrangian remapping contains three steps, each with their own errors. (1) The 'original' positions of the (4 or 6) corner points are found by integrating backward in time: *integration* errors. (2) The corner points are connected with straight lines instead of the curved sides of the pre-image: *representation* errors. (3) This polygon is intersected with the (piecewise) polynomial approximation of the liquid interface at the previous time step: *reconstruction* errors.

When the time step satisfies a CFL-condition while a second-order time-integration method is used, it can be shown [9, 10] that the reconstruction errors in the position of the interface are the larger of the three: $\mathcal{O}(h^p)$, where p is the order of the approximation ($p = 2$ for a piecewise linear approximation, and $p = 3$ for a parabolic approximate). We will illustrate this in the simulations in Sect. 5.1.

Discrete donating regions The mentioned errors jeopardize the exact discrete conservation properties of the numerical scheme: the amount of liquid moved may not match the fluxes through the faces of the control volume. This makes Lagrangian remapping not good enough for our discrete conservation wishes, which not only influences a correct energy balance but also numerical stability. An alternative approach is to consider the pre-image of the *individual faces* of a cell, and the region between the pre-image and the face, which corresponds with the liquid that passes through the face: the *donating region* red(DR) [9]. Now, corrections can be applied which match the area of the donating region to the amount fluxed through the face, and thus discrete conservation can be retained [11].

It is natural to demand that the total amount of liquid inside a cell χ remains between 0 and 1, i.e. no wisps or 'flotsam and jetsam' [12]. Also, it should be prevented that the same liquid is fluxed through two different faces. This yields restrictions to the construction of the donating regions. Owkes and Desjardins [13] introduced a suitable method as an ingeneous extension to the edge-matched flux polygon advection (EMFPA) method [14], which is an unsplit DR-based advection method. It introduces a fifth vertex of the DR, see Fig. 5, giving sufficient flexibility to satisfy the requirements for a DR. We will call this modification the MEMFPA method; it is our method of choice.

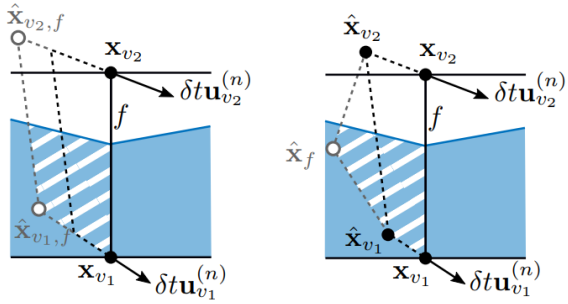

(a) EMFPA. (b) MEMFPA.

FIGURE 5. TWO-DIMENSIONAL DONATING REGIONS WITH AN (EXAGGERATED) CORRECTION.

3.2 Mass fluxes

Because the mass fluxes also feature in the momentum fluxes we give some notation. Firstly, the region covered by phase π at time level (n) is denoted by $\Omega^{\pi,(n)}$. Next, the donating region of the flow that passes a face f over a time interval δt is denoted by $\Delta_f^{(n)}$. In the discrete one-velocity setting, this region is determined by the velocity $\boldsymbol{u}$ at the cell face f. The amount of phase π present in this DR, indicated by Λ_0^{π}, equals the amount of that phase that

crosses this face over the time interval:

$$\mathfrak{m}_f^{\pi,(n)}\delta t = \rho^\pi \Lambda_0^\pi\big(\Delta_f(\boldsymbol{u}^{(n)}) \cap \Omega^{\pi,(n)}\big), \tag{7}$$

where a positive-sign means a mass flux in positive direction. Eq. (7) is the discrete equivalent of the contour integral in Eq. (1) integrated over the time interval $[t^{(n)}, t^{(n+1)}]$.

Adding, with the appropriate signs, these mass fluxes over all faces of a cell gives the change over the time interval δt of the amount of phase π present in the cell. With the MEMFPA method the new amount of liquid in the cell satisfies all requirements for the VOF function. For the one-velocity model, the above approach leads to a sharp definition of the interface, with discrete mass conservation for each of the phases.

Two-velocity model In the two-velocity model, the velocity field around the free interface is not smooth, with liquid velocities u^l on one side and gas velocities u^g on the other side. Moreover, only the mixed velocity field has been made divergence-free following Eq. (5) (see Sect. 3.4), and not the individual velocity fields. For advecting the liquid we want to use a smooth, divergence-free, extension of the liquid velocity filed into the gas domain. This GFM-like extension is provided through the solution of an auxiliary pressure Poisson problem, and leads to a liquid velocity field denoted by $\widehat{\boldsymbol{u}}^l$. With this smooth velocity field the donating regions around the free interface are constructed, leading to $\widehat{\Delta}^l \equiv \Delta(\widehat{\boldsymbol{u}}^l)$. This region is then used in the mass flux (7), and leads to perfect mass conservation.

3.3 Advection of momentum

In a staggered grid, the velocity components are defined at cell faces, whereas the discussion in the previous subsection is applicable to variables defined in cell centers. A control volume for the conservation of momentum is shown as the green-colored rectangle in Fig. 3, covering half the adjacent primary grid cells for mass conservation. This intimate connection goes even further when one not only wants mass and momentum conservation, but also conservation of kinetic energy. This connection has been studied in [15] for incompressible flow and in [16] for compressible flow (also covering multi-phase flow). It is shown that discrete energy is conserved when the conservation balance for the (green in Fig. 3) momentum volume is taken as half the balance for the sum of the (red) partially-overlapping mass volumes. In that case, the fluxes required are those along the faces of the mass control volumes, i.e., the mass fluxes through the red faces in Fig. 3. In fact, this condition is necessary when discrete energy conservation is desired [16, 17].

The finite-volume discretization of momentum conservation then uses a momentum flux per time unit at the location e (see Fig. 3) given by (cf. Eq. (7))

$$\mathfrak{m}_e^\pi u_{\mathrm{DR}}^\pi, \;\text{ with }\; \mathfrak{m}_e^\pi = \tfrac{1}{2}\big(\mathfrak{m}_C^\pi + \mathfrak{m}_E^\pi\big). \tag{8}$$

Here, u_{DR}^π is a value representative for the DR of the π phase. It could be taken as the value in the centroid of the DR, but also it could be taken as $\frac{1}{2}\big(u_C^\pi + u_E^\pi\big)$. The former choice gives a stabilizing upwind character, while the latter choice corresponds with an energy-preserving central discretization [16].

One-velocity model Near the interface, the above procedure will produce two velocity values u^l and u^g, which in general will not be equal. To combine them into one we follow [18] and define a single continuous velocity via the mass-weighted sum of the momentums

$$\bar{u}^{(n+1)} = \frac{(\chi\rho u^{(n+1)})^l + (\chi\rho u^{(n+1)})^g}{(\chi\rho)^l + (\chi\rho)^g}. \tag{9}$$

It yields exact conservation of total linear momentum.

Two-velocity model In the two-velocity approach, for the advection of the liquid momentum in Eq. (8) we use the extrapolated liquid velocity $\widehat{u}^l$ for which the divergence vanishes as discussed above. This implies that for the liquid linear momentum is exactly conserved.

For the gas phase we use the gas velocity field u^g. As the gas volume fraction has been chosen as the complement of the liquid fraction (and not constructed via a gaseous DR), gas linear momentum is not exactly conserved. But, as the liquid is much heavier than the gas, conservation of liquid momentum is far more important.

3.4 The pressure Poisson equation

Next we discuss the pressure Poisson problem, which arises from imposing the divergence constraint, to which

we add the jump conditions imposed by Eqs. (4) and (6). This Poisson problem is constructed from the discrete form of combined mass conservation in Eq. (5), thus assuring that each primary cell stays filled with fluid (liquid and/or gas). As usual, the face velocities are replaced by a local discrete momentum equation (2), thus turning the mixed mass conservation (5) into a Poisson equation for the pressure.

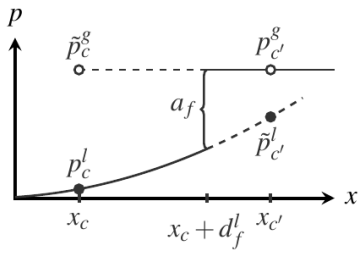

FIGURE 6. ILLUSTRATION OF THE GHOST FLUID METHOD (GFM) TO HANDLE THE JUMPS IN THE PRESSURE AND ITS GRADIENT.

In Liu et al. [19] the ghost fluid method (GFM) is introduced for computing a derivative in the presence of value and derivative jumps Eqs. (4) and (6). We use a multi-dimensional generalisation of the GFM [10]. Fig. 6 shows how both sides of the pressure are provided with a ghost point. For these two ghost values, two equations are available: the two jumps just-mentioned.

Capillary effects The above advection method leads to a new liquid distribution, described by an updated VOF-function. The free surface is derived from the VOF-function by means of a (generalized) local height function (G)LHF [20–22]. From this local height function the curvature can be computed, which involves taking a second-order derivative in which we have to divide by h^2. However we have seen in Sect. 3.1 that the accuracy of the position of the surface, i.e. of the height function, is only second order when a linear reconstruction of the surface is used. In that case we may expect that the error in the curvature is of order zero, hence it may not become smaller under grid refinement. Therefore, in applications where capillary effects, i.e. the curvature, plays a dominant role, we advise to opt for a piecewise parabolic reconstruction of the free surface. We will demonstrate this in the examples below.

4 Comparison with other approaches

Tab. 1 gives an overview of momentum transport methods found in the literature, restricted to staggered formulations using a DR-based geometric VOF method. Our proposed advection method for both the one- and two-velocity formulation has been included. In the dimensionally unsplit method from [13] a CTU (corner transport upwind) flux interpolant [25] is used in a neighborhood around the interface. Because it is rather diffusive, we use the CTU flux interpolant as little as possible. It seems that the proposed equally-weighted volume fluxes result in the only (split or unsplit) momentum transport method which does not require any additional volume flux computation. The method sharply models the interface, and exactly mass and momentum conservative for the liquid phases in both formulations. For the gaseous phase, mass is also conserved, while momentum is conserved for the one-velocity formulation.

An impression of the difference in accuracy between the one-velocity and two-velocity models can be inferred from Fig. 7. It shows three detailed snapshots of simulations of a breaking wave from [26], which will lead to a large gas-pocket impact (LGPI) a few moments later. We give more results in Sect. 5.3. The first two snapshots show the results on a very fine grid and on a 16× coarser grid (3.1mm versus 0.2mm) with the one-velocity method. The

	Unsplit?	Conservative momentum?	# volume fluxes	# velocities	Flux interpolation
Rudman et al. [23]	N	$l+g$	$d2^{d-1}$	1	Flux limiting
Zuzio et al. [24]	N	$l+g$	$d2^{d-1}$	1	WENO5
Arrufat et al. [18]	N		d^2	1	QUICK/Superbee
Owkes et al. [13]	Y	$l+g$	$d2^{d-1}$	1	CTU near interface
One-velocity	Y	$l+g$	0	1	CTU if needed
Two-velocity	Y	l	d	2	CTU if needed

TABLE 1. EXISTING ONE-VELOCITY MODELS VERSUS OUR ONE- AND TWO-VELOCITY MODELS: '$l+g$' = THE SUM OF LIQUID AND GAS MOMENTUM IS CONSERVED; 'l' = ONLY LIQUID MOMENTUM IS CONSERVED.

very fine grid shows small flow details, but the coarse grid shows a very thick, unphysical boundary layer. In contrast, on this same coarse grid the two-velocity method shows a smooth velocity field, apart from flow details, similar to the results on the 16× finer grid.

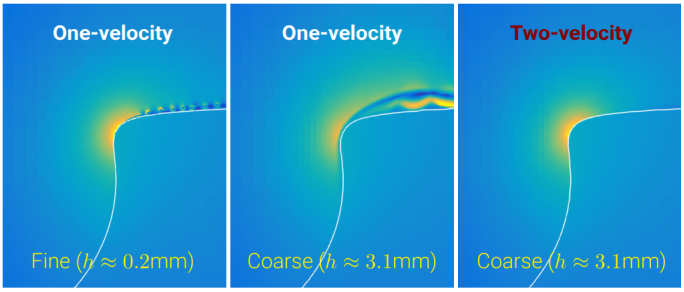

FIGURE 7. SNAPSHOTS FROM A LARGE GAS-POCKET IMPACT [26] AT $t/T^g \approx 1.27$ (where $T^g = (L/g)^{1/2}$) AND SCALE $1:5$ ($L = 4$m). IT COMPARES THE TWO-VELOCITY MODEL ON A COARSE GRID WITH THE ONE-VELOCITY MODEL ON THE SAME COARSE GRID AND ON A MUCH FINER ONE. COLORS REPRESENT VELOCITY CLIPPED TO $|\boldsymbol{u}|_2 \in [0, 10]$.

5 Examples

5.1 Vortex reverse

As a first example, the time-dependent accuracy of the proposed interface advection and reconstruction methods is evaluated using the classical vortex reverse problem [27] where the interface undergoes a reversible deformation. The piecewise linear approximation of the interface will be based on existing PLIC methods, like ELVIRA [28,29] and MoF [30]. Their generalizations to piecewise parabolic approximation we have named PLVIRA and PMoF.

In Fig. 8 we show the accuracy in the computed curvature under grid refinement: the PLIC methods do not lead to a convergent curvature, as can be explained from the discussion in Sect. 3.4. The PMoF method yields a first-order accurate curvature, which we expected from the aforementioned discussion. Interestingly, the PLVIRA and PROST methods even yield a second-order accurate curvature, which we cannot yet explain rigorously.

Another positive effect of the parabolic reconstruction is the huge reduction in spurious (parasitic) currents, as

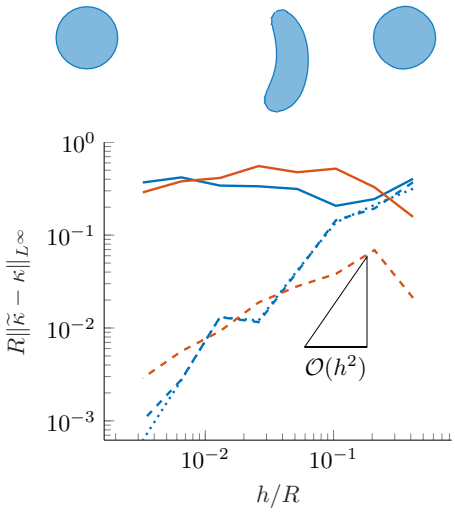

FIGURE 8. ACCURACY OF THE CURVATURE FOR THE VORTEX REVERSE PROBLEM AT $t = T$. IN BLUE THE RESULTS FOR (P)LVIRA AND IN RED FOR (P)MoF, WITH THE LINEAR VERSIONS SOLID AND THE PARABOLIC VERSIONS DASHED.

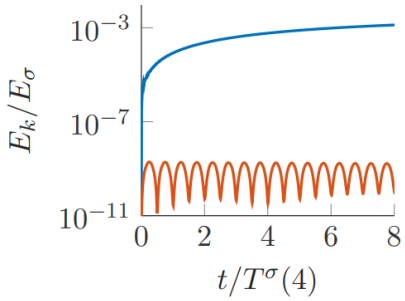

FIGURE 9. SPURIOUS VELOCITY ERRORS FOR PIECEWISE LINEAR (IN BLUE) AND PIECEWISE PARABOLIC (IN RED) RECONSTRUCTION.

shown in Fig. 9. Therefore, in applications where capillary effects, i.e. the curvature, plays a dominant role, we advise to opt for a piecewise parabolic reconstruction of the free surface.

5.2 Droplet pinch-off

As a practical example where capillary effects play an essential role, Fig. 10 shows some snapshots of a capillary pinch-off of droplets from a long liquid filament [31]. The plots also give an indication of the adaptive mesh refinement (AMR) [7] around the pinch-off position.

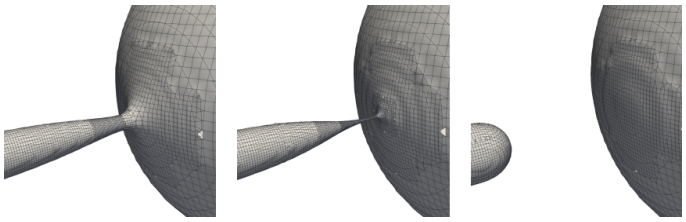

FIGURE 10. CLOSE UP OF DROPLET PINCH-OFF WITH THE TWO-VELOCITY MODEL.

5.3 Breaking waves

Fig. 11(a) shows some simulation snapshots (with the two-velocity model) of the breaking of a Stokes-3 wave. In the first (top) snapshot, the velocity profile in the escaping gas in front of the wave tip is also shown. Fig. 11(b) shows a grid-refinement study of the plunging breaker, in which the levels of refinement are increased from 4 to 6. The reference solution is obtained with even further refinement. Also, as a dashed curve, results from the one-velocity model are shown.

Finally, we turn to the example shown in the introductory section: a large gas-pocket impact (LGPI), resulting in the impact of a 4m long wave. We do not aim at entirely resolving the interface layer, since this would be too expensive. Fig. 12 shows some preliminary results for emerging instabilities when the tip of a breaking wave is close to the wall. In particular, we study the influence of capillary effects via the scale with which the wave is investigated. It is to be expected that when the scales increases, i.e. the model becomes smaller, the more influential the capillary effects are going to be. In other words, at larger scales a smoother surface can be expected. This is indeed confirmed in Fig. 12(b), which shows details shortly before impact against the tank wall. The simulations at scale 1:40 show a smooth wave tip, but at scales 1:20 and 1:10 irregularities at the surface can be seen which (probably) have a physical meaning and are not due to numerical instabilities.

redThis example illustrates our contribution to the SLING project. It is our task to demonstrate that the visible instabilities are of physical origin, and not artefacts due to flaws in the numerical scheme. To validate our results, elsewhere in the project a series of experiments has been carried out - a comparison between the two sets of results will follow later. Ultimately, the influence on the wave impacts against the containment walls will be further investigated.

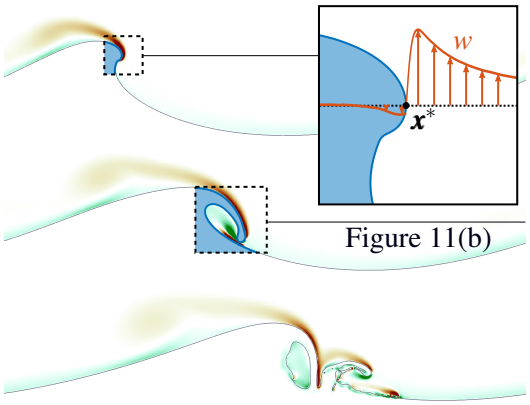

(a) Vorticity and interface profile at $t/T^g \approx 0.52$, 0.66 and 0.8.

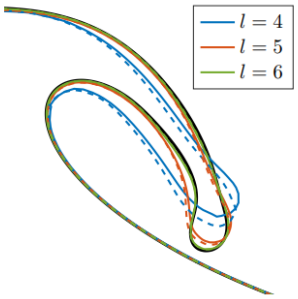

(b) Convergence under local refinement of interface profile at $t/T^g \approx 0.66$.

FIGURE 11. (a) BREAKING WAVE COMPUTED WITH THE TWO-VELOCITY MODEL. (b) THE DASHED AND SOLID LINES CORRESPOND TO THE ONE- AND TWO-VELOCITY MODEL, RESPECTIVELY. IN SOLID BLACK A REFERENCE SOLUTION ON A MUCH FINER GRID.

6 Conclusion

We have proposed the use of a two-velocity formulation for simulating two-phase Navier–Stokes equations. To conserve mass and momentum in a sharp and accurate way, we use the same approximate space-time integration of the advection equation for momentum as is used for the advection of mass [16, 17]. For the one- and two-velocity formulations the liquid mass and linear momentum are conserved exactly. Capillary effects have been modelled with a jump in the pressure. A parabolic reconstruction of the interface is proposed for grid convergence, which also highly reduces parasitic currents. The proposed method is shown to converge for reversible deformation test cases. Examples of a breaking wave show that the one-velocity formulation yields low accuracy for the lighter of the two phases, but

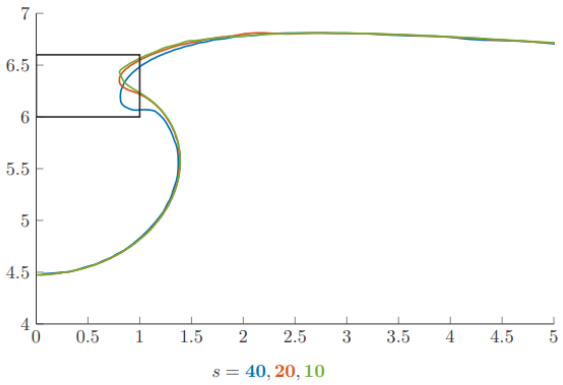

(a) Global view.

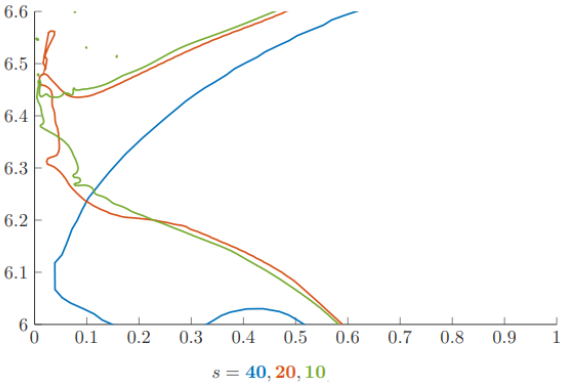

(b) Details near tank wall.

FIGURE 12. WAVE TONGUES SHORTLY BEFORE IMPACT. ON THE SMALLER SCALES, INSTABILITIES ARE DEVELOPING.

using the two-velocity formulation results in good accuracy for both phases. redCurrently, the new two-phase approach is being implemented in the ComFLOW program, and is planned to be available in its next release.

7 ACKNOWLEDGMENTS

This work is part of the research programme SLING, which is (partly) financed by the Netherlands Organisation for Scientific Research (NWO). We would like to thank the Center for Information Technology of the University of Groningen for their support and for providing access to the Peregrine high performance computing cluster. Moreover we thank dr. Joaquin López for kindly providing the VoFTools library.

REFERENCES

[1] Lafeber, W., Brosset, L., and Bogaert, H., 2012. "Comparison of wave impact tests at large and full scale : Results from the Sloshel project". In 22nd International Symposium on Offshore and Polar Engineering, Vol. 4, pp. 285–299.

[2] Saurel, R., and Abgrall, R., 1999. "A multiphase Godunov method for compressible multifluid and multiphase flows". *Journal of Computational Physics,* ***150***(2), pp. 425–467.

[3] Arakawa, A., 1966. "Computational design for long-term numerical integration of the equations of fluid motion: Two-dimensional incompressible flow. Part I". *Journal of Computational Physics,* ***1***, pp. 119–143.

[4] Kleefsman, K. M. T., Fekken, G., Veldman, A. E. P., Iwanowski, B., and Buchner, B., 2005. "A Volume-of-Fluid based simulation method for wave impact problems". *Journal of Computational Physics,* ***206***, pp. 363–393.

[5] Wemmenhove, R., Luppes, R., Veldman, A. E. P., and Bunnik, T., 2015. "Numerical simulation of hydrodynamic wave loading by a compressible two-phase flow method". *Computers and Fluids,* ***114***, pp. 218–231.

[6] Düz, B., Borsboom, M. J. A., Wellens, P. R., Veldman, A. E. P., and Huijsmans, R. H. M., 2017. "An absorbing boundary condition for free-surface water waves". *Computers and Fluids,* ***156***, pp. 562–578.

[7] van der Plas, P., 2017. "Local grid refinement for free-surface flow simulations". PhD thesis, University of Groningen.

[8] Zinjala, H. K., and Banerjee, J., 2015. "A Lagrangian-Eulerian Volume-Tracking with Linearity-Preserving Interface Reconstruction". *Numerical Heat Transfer, Part B,* ***68***, pp. 459–478.

[9] Zhang, Q., 2013. "On a family of unsplit advection algorithms for volume-of-fluid methods". *SIAM Journal on Numerical Analysis,* ***51***(5), pp. 2822–2850.

[10] Remmerswaal, R. A., and Veldman, A. E. P., 2021. "Parabolic interface reconstruction for 2D volume of fluid methods". *arXiv preprint arXiv:2111.09627.*

[11] Remmerswaal, R. A., and Veldman, A. E. P., 2022. "A sharp two-velocity model for two-phase flow. Part I. Transport of mass and momentum.". In preparation.

[12] Rider, W. J., and Kothe, D. B., 1995. Stretching and

tearing interface tracking methods. AIAA paper 95-1717.

[13] Owkes, M., and Desjardins, O., 2017. "A mass and momentum conserving unsplit semi-Lagrangian framework for simulating multiphase flows". *Journal of Computational Physics,* ***332***, pp. 21–46.

[14] Lopez, J., Hernandez, J., Gomez, P., and Faura, F., 2004. "A volume of fluid method based on multidimensional advection and spline interface reconstruction". *Journal of Computational Physics,* ***195***, pp. 718–742.

[15] Droge, M., and Verstappen, R., 2005. "A new symmetry-preserving Cartesian-grid method for computing ow past arbitrarily shaped objects". *International Journal for Numerical Methods in Fluids,* ***47***, pp. 979–985.

[16] Veldman, A. E. P., 2021. "Supraconservative finite-volume methods for the Euler equations of subsonic compressible flow". *SIAM Review,* ***63***, pp. 756–779.

[17] Veldman, A. E. P., 2019. "A general condition for kinetic-energy preserving discretization of flow transport equations". *Journal of Computational Physics,* ***398***, p. 108894. doi:10.1016/j.jcp.2019.108894.

[18] Arrufat, T., Crialesi-Esposito, M., Fuster, D., Ling, Y., Malan, L., Pal, S., Scardovelli, R., Tryggvason, G., and Zaleski, S., 2021. "A mass-momentum consistent, Volume-of-Fluid method for incompressible flow on staggered grids". *Computers and Fluids,* ***215***, p. 104785.

[19] Liu, X.-D., Fedkiw, R. P., and Kang, M., 2000. "A boundary condition capturing method for Poisson's equation on irregular domains". *Journal of Computational Physics,* ***160***, pp. 151–178.

[20] Gerrits, J., 2001. "Dynamics of liquid-filled spacecraft: numerical simulation of coupled solid-liquid dynamics". PhD thesis, University of Groningen.

[21] Gerrits, J., and Veldman, A. E. P., 2003. "Dynamics of liquid-filled spacecraft". *Journal of Engineering Mathematics,* ***45***, pp. 21–38.

[22] Popinet, S., 2009. "An accurate adaptive solver for surface-tension-driven interfacial flows". *Journal of Computational Physics,* ***228***(16), pp. 5838–5866.

[23] Rudman, M., 1998. "A volume-tracking method for incompressible multifluid flows with large density variations". *International Journal for Numerical Methods in Fluids,* ***28***(2), pp. 357–378.

[24] Zuzio, D., Orazzo, A., Estivalèzes, J.-L., and Lagrange, I., 2020. "A new efficient momentum preserving level-set/vof method for high density and momentum ratio incompressible two-phase flows". *Journal of Computational Physics,* ***410***, p. 109342.

[25] Leveque, R. J., 1996. "High-Resolution Conservative Algorithms for Advection in Incompressible Flow". *SIAM Journal on Numerical Analysis,* ***33***(2), pp. 627–665.

[26] Etienne, S., Scolan, Y.-M., and Brosset, L., 2018. "Numerical study of density ratio influence on global wave shapes before impact". In International Conference on Offshore Mechanics and Arctic Engineering, Vol. 51302, American Society of Mechanical Engineers, p. V009T13A025.

[27] Rider, W. J., and Kothe, D. B., 1998. "Reconstructing volume tracking". *Journal of Computational Physics,* ***141***, pp. 112–152.

[28] Puckett, E. G., 1991. "A volume-of-fluid interface tracking algorithm with applications to computing shock wave refraction". In Proceedings of the Fourth International Symposium on Computational Fluid Dynamics, pp. 933–938.

[29] Pilliod, J. E., and Puckett, E. G., 2004. "Second-order accurate volume-of-fluid algorithms for tracking material interfaces". *Journal of Computational Physics,* ***199***(2), pp. 465–502.

[30] Dyadechko, V., and Shashkov, M., 2005. "Moment-of-fluid interface reconstruction". *Mathematical Modeling and Analysis,* ***836***, pp. 1–41.

[31] Remmerswaal, R. A., and Veldman, A. E. P., 2022. "A sharp two-velocity model for two-phase flow. Part II. The Poisson problem.". In preparation.